Asian Journal of Chemistry; Vol. 35, No. 9 (2023), 2197-2202

ASIAN JOURNAL OF CHEMISTRY

https://doi.org/10.14233/ajchem.2023.28123

Enhanced Acetone Gas Sensing Properties of Al-Doped ZnO Thin Films Developed by Sol-Gel Dip Coating Method

C. RAJAN*, N. PASUPATHY, R. MURUGESAN and J. GOBINATH

Department of Electronics, Research and Development Centre, Erode Arts and Science College (Autonomous), Erode-638009, India

*Corresponding author: E-mail: mankalairajan@gmail.com

Received: 8 June 2023; *Accepted*: 24 July 2023; *Published online*: 31 August 2023; AJC-21364

The acetone sensing capabilities of pure and Al-doped ZnO thin films developed by the sol-gel dip coating technique were examined in this study. An investigation was conducted to examine the impact of Al doping concentration on the structural, morphological and sensing characteristics of the films. The results showed that acetone gas detection in ZnO thin films might be enhanced by doping with Al. In particular, when exposed to 10 ppm of acetone at room temperature, the response of 3 at% Al-doped ZnO thin film was the highest, achieving 53% and showed a fast response time of 6 s and a recovery time of 32 s. The researchers conducted additional investigations into the selectivity of acetone in the film when exposed to various interfering gases. The results revealed that acetone exhibited a favourable level of selectivity. The results presented herein demonstrate the effectiveness of sol-gel dip-coated thin films of Al-doped ZnO in the context of acetone gas sensing applications.

Keywords: Acetone sensing, Sol-gel dip coating, Al doping, Thin films, Gas sensing.

INTRODUCTION

The volatile organic compound acetone is generated as a byproduct of metabolic processes within the human body. Recent research findings have revealed that individuals suffering with diabetes exhibit the elevated levels of a certain substance in their exhaled breath. This observation suggests that the aforementioned substance holds promise as a potential biomarker for the purpose of diagnosing diabetes [1]. For the diagnosis and monitoring of diabetes, it is essential to develop effective and selective acetone sensors. Due to its high sensitivity, low cost and ease of fabrication, zinc oxide is a potential material for acetone sensing [2]. The sensing capabilities of ZnO thin films towards several gases, including acetone, have been found to be improved by Al doping [3].

Due to its special characteristics, including a high surface-to-volume ratio, high sensitivity and high stability, ZnO has been extensively studied as a sensing material for several gases [4]. However, by doping ZnO with various elements, the sensitivity and selectivity of ZnO towards particular gases can be further enhanced [5]. Due to its low toxicity and inexpensive cost, aluminum is one of the most often utilized dopants for ZnO thin films [6].

Numerous investigations showed how Al doping improves the sensing capabilities of ZnO thin films towards acetone gas. Al-doped ZnO thin films were found to be more sensitive to acetone than pure ZnO thin films [7]. Furthermore, it has been observed that Al doping increased the sensitivity and selectivity of ZnO thin films towards acetone gas [8].

An efficient way to develop ZnO thin films is the sol-gel dip coating method. This approach has a number of advantages, including low cost, low processing temperature and good repeatability [9]. Therefore, in this study, we prepared pure and Al-doped ZnO thin films using the sol-gel dip coating process and examined their acetone gas sensing capabilities. The present study aimed to evaluate the influence of Al doping on the structural, morphological, and sensing properties of thin films. The findings revealed that the incorporation of Al into ZnO thin films resulted in an enhancement of their sensing capacities towards acetone gas. The 3 at% Al-doped ZnO thin film demonstrated the best response to 10 ppm of acetone at room temperature, demonstrating its potential for the acetone gas sensing applications.

EXPERIMENTAL

A 0.2 M solution of $Zn(CH_3COO)_2{\cdot}2H_2O$ was prepared by dissolving 0.746 g of $Zn(CH_3COO)_2{\cdot}2H_2O$ in 20 mL of ethanol, similarly 0.02 M solution of $Al(NO_3)_3{\cdot}9H_2O$ was prepared by dissolving 0.026 g of compound in 20 mL of ethanol. Now diethanolamine was added dropwise to a ZnO solution while being constantly stirred until the pH reached 7. The necessary concentration of aluminium was obtained for Al-doped ZnO thin films by combining the appropriate volume of aluminium nitrate solution with ZnO solution. To prepare 3 at% Al-doped ZnO, for instance, 17 mL of ZnO solution was mixed appropriately with 3 mL of aluminium nitrate solution using magnetic stirrer for a further 2 h.

Following a series of 10 min sonication in acetone, ethanol and deionized water, glass substrates were dried with nitrogen gas. The clean substrates were vertically dipped into the solution and withdrawn at a speed of 5 mm/s by using an automatic dip coating machine. The substrates with coatings underwent a drying process at a temperature of 100 ºC for 10 min, allowing the solvent to evaporate. Subsequently, they were annealed in air at 500 ºC for 2 h, resulting in the formation of thin films of ZnO and Al-doped ZnO.

Characterization: X-ray diffraction (XRD) and scanning electron microscopy (SEM) were used to determine the structural and morphological characteristics of the films. The optical characteristics of the produced films were examined using a UV-vis spectrometer. The gas sensing capabilities of the thin films were evaluated using a specifically constructed gas sensing apparatus. The electrical resistance of the thin films was evaluated while they were subjected to acetone gas at various concentrations (1 ppm to 25 ppm). The response time and recovery times of the prepared thin films were also observed.

RESULTS AND DISCUSSION

XRD studies: To ascertain the structural characteristics of the films, an X-ray diffractometer with high resolution and a Cu*K*α radiation source was used for the XRD investigation. The diffraction patterns were captured with a step size of 0.02º in the 2θ range of 20º to 80º. Pure ZnO, ZnO doped with 1 at% Al, ZnO doped with 3 at% Al and ZnO doped with 5 at% Al are the four distinct samples of ZnO with aluminium doping. The common names for these samples are AZO-0%, AZO-1%, AZO-3% and AZO-5%, respectively. According to the XRD results (Fig. 1), each sample possessed a hexagonal wurtzite structure, which was demonstrated by the sharp (002) diffraction peak at 2θ = 34.42º, which is consistent with the ZnO *c*-axis orientation.

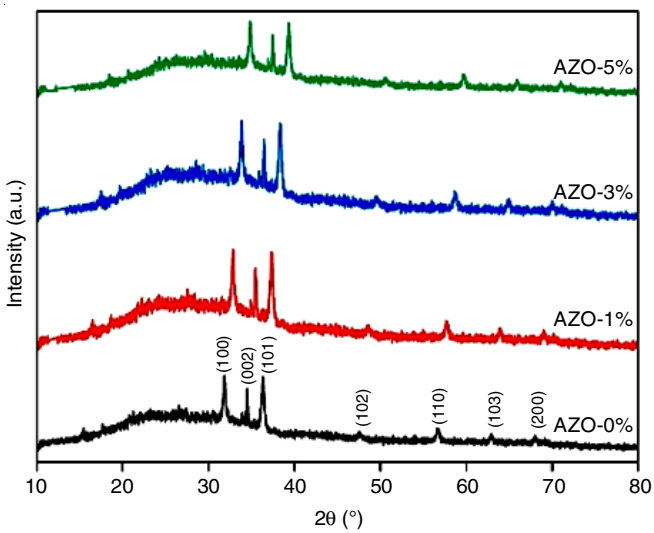

Fig. 1. XRD pattern of pure and Al doped ZnO films

Table-1 listed the observed diffraction peak angles and related crystallographic planes for a range of doping concentrations. The Joint Committee on Powder Diffraction Standards (JCPDS) card no. 36-1451 was used to identify the diffraction peaks. With increasing Al doping concentration, the XRD patterns also revealed a minor shift in the diffraction peaks towards higher angles, indicating the incorporation of Al ions into the ZnO lattice [10]. The difference in ionic radii between Zn^{2+} (0.74 Å) and Al^{3+} (0.53 Å), which causes lattice strain and a minor drop in the lattice constant of ZnO [11], is responsible for the shift in the diffraction peaks. The Scherrer's equation was used to calculate the average crystallite size of the thin films from the full width at half maximum (FWHM) of the (002) peak. For pure ZnO and ZnO with Al doping, the crystallite size was determined to be in the range of 27.1 to 32.5 nm and 26.3 to 30.1 nm, respectively. A decrease in crystallite size with increasing Al doping concentration is attributed to the reduction in grain growth resulting from the introduction of Al ions [12].

SEM studies: A scanning electron microscope (SEM) was used to analyze the surface morphology of the thin films. The images were obtained at a magnification of 5000x and an accelerating voltage of 15 kV. The SEM images of pure ZnO and Al-doped ZnO thin films (Fig. 2) revealed a consistent, dense and hexagonal-shaped surface morphology. The absence of cracks or gaps in the surface morphology of the films demonstrated the successful production of continuous thin films. Using ImageJ software, the surface roughness of the films was calculated, with pure ZnO having an average roughness value of 10 nm and Al-doped ZnO thin films having an average roughness value of 12 nm. The inclusion of Al ions, which causes a modest

TABLE-1
DOPING CONCENTRATION, CRYSTALLOGRAPHIC PLANES AND DIFFRACTION ANGLES FOR ZnO AND AZO FILMS

Doping concentration	Crystallographic planes						
	(100)	(002)	(101)	(102)	(110)	(103)	(200)
Pure ZnO	31.82°	34.42°	36.31°	47.60°	56.71°	62.91°	67.92°
AZO-1%	32.86°	35.45°	37.34°	48.49°	57.66°	63.90°	68.97°
AZO-3%	33.85°	36.47°	38.39°	49.62°	58.62°	64.86°	69.93°
AZO-5%	34.88°	37.41°	39.38°	50.64°	59.63°	65.83°	70.94°

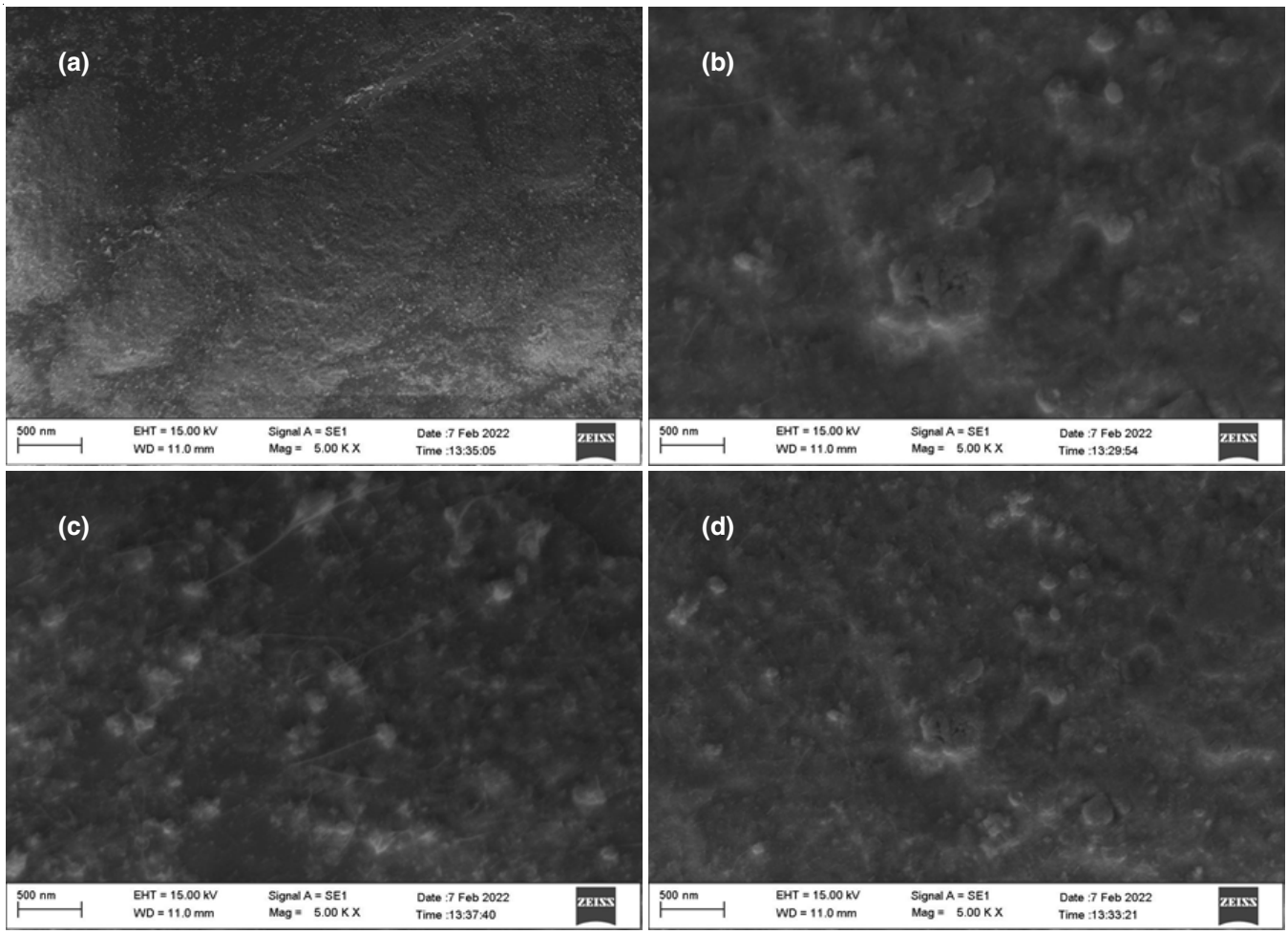

Fig. 2. SEM images of (a) AZO-0% (b) AZO-1% (c) AZO-3% (d) AZO-5%

rise in surface roughness, is responsible for the increase in the roughness for the Al-doped ZnO films [13].

Using ImageJ software, the grain size distribution of the thin films was calculated from the SEM images. For pure ZnO and Al-doped ZnO, the grain size was determined to be in the range of 20 to 50 nm and 18 to 45 nm, respectively. The reduction in grain growth caused by the incorporation of Al ions is what causes the decrease in grain size with increasing Al doping concentration [14].

Ultra-violet absorption: A UV-Vis spectrophotometer was used to perform UV-Vis spectroscopy in the range of 200 to 800 nm wavelength. Pure ZnO and Al-doped ZnO thin films both have distinctive UV absorption edges and visible transparency ranges in their UV-Vis spectra [15]. The absorption edge is mostly attributed to the electrical transitions of the material from the valence band to the conduction band. The absorbance graph is shown in Fig. 3.

With increasing Al doping concentration, the absorption edge of the films exhibits a shift towards longer wavelengths (redshift) [16]. This suggests that the inclusion of Al ions into the ZnO lattice has caused a reduction in the bandgap energy of the films [17]. The redshift phenomenon can be attributed to the introduction of Al dopants, which give rise to intermediate energy levels inside the bandgap. The optical absorption properties and bandgap energies of thin films play a crucial role in their applications in sensing. The Al-doped ZnO thin films are suitable for acetone sensing as they permit higher sensitivity in the necessary wavelength range due to the redshift in the absorption edge (Fig. 4) and the tunability of the bandgap energy by Al doping [18].

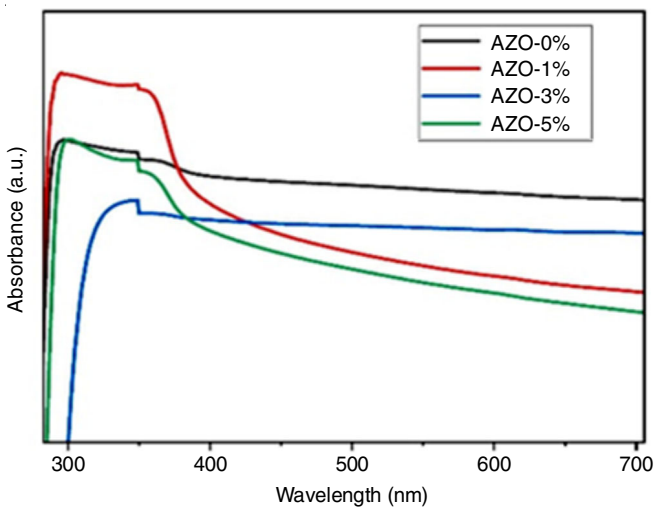

Fig. 3. UV-Vis absorption spectra of pure and Al doped ZnO thin films

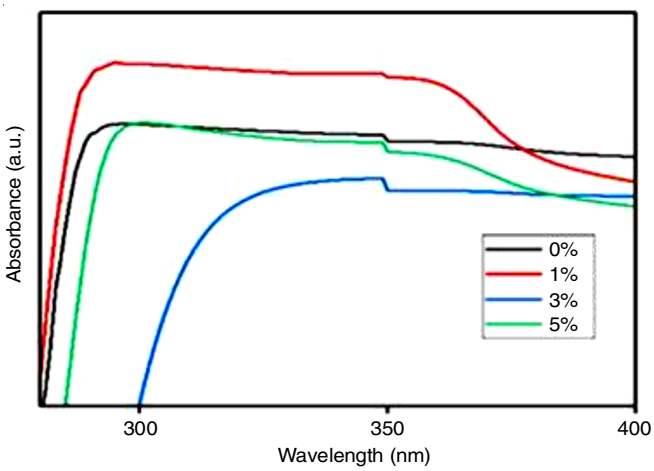

Fig. 4. Red shift behavior in pure and Al doped ZnO thin films

Band gap: The Tauc plot can be used to determine the bandgap energy (E_g) of the films. The bandgap energy of pure ZnO thin film was found to be 3.17 eV, whereas the bandgap energies were found to be 3.15 eV and 3.08 eV, respectively, for Al-doped ZnO thin films with an Al concentration of 1% and 3% (Fig. 5). As Al doping concentration increases, the bandgap energy decreases, indicating the formation of an alloyed ZnO:Al.

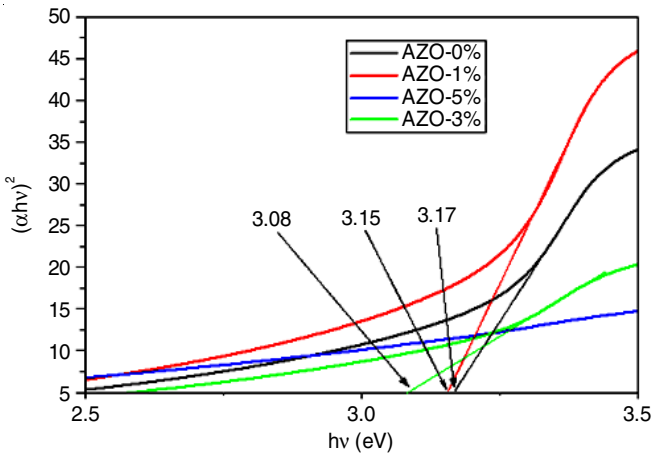

Fig. 5. Band gap variation of pure and Al doped ZnO thin films

Acetone gas sensing response: When exposed to various concentrations of acetone gas (pure, 1 at%, 3 at% and 5 at%), the change in electrical resistance of pure and Al-doped ZnO thin films was determined. The outcomes showed a definite influence of Al doping on the acetone sensing capabilities of the films. The sensing performance of the thin films at various acetone gas concentrations is shown in Fig. 6. Upon exposure to acetone gas, the electrical resistance of the films exhibited a significant decrease, indicating an enhanced conductivity resulting from the interaction between acetone molecules and the surface of the film. The charge transfer mechanisms and surface reactions that take place when acetone molecules are adsorbed onto the film surface are responsible for this change in resistance [19].

Among all the samples, 3% Al-doped ZnO thin film demonstrated the highest response, displaying a greater reduction in resistance compared to the pure and other Al-doped films. Al ions are incorporated into the ZnO lattice, causing defects and increasing the amount of acetone adsorption sites, which results in this improved response. The response was determined as the percentage change in resistance using the following formula to assess the sensitivity of the thin films to acetone gas:

$$\text{Response } (\%) = \frac{R_o - R_{gas}}{R_o} \times 100$$

where R_{gas} is the film's resistance in the presence of acetone gas and R_o is the film's initial resistance.

When exposed to 10 ppm of acetone at room temperature, 3% Al-doped ZnO thin film showed the maximum sensitivity to acetone gas, with a response of 53%. This shows the film's strong sensitivity to the target gas and its capacity to identify acetone gas at low concentrations. By subjecting the thin films to various interfering gases, such as ammonia, methanol, ethanol and isopropanol, the selectivity of the thin films towards acetone was evaluated. The findings demonstrated the good selectivity of the film for acetone and low sensitivity to interfering gases (Fig. 7). This selectivity is essential in real-world applications where it is necessary to detect and distinguish between particular target gases.

To evaluate the dynamic performance of the thin films, the response and recovery times were assessed. The reaction time

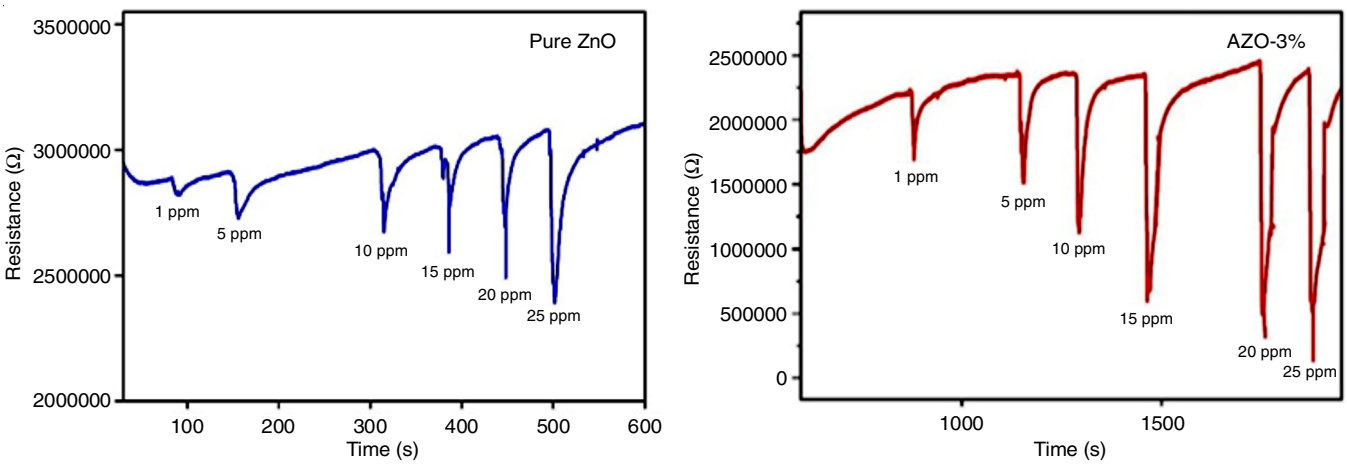

Fig. 6. Sensing performance of pure and AZO-3% films

TABLE-2
A COMPARISON OF ACETONE DETECTION IN THE CURRENT STUDY AND PUBLISHED WORK

Material	Method	Temperature (° C)	Acetone (ppm)	Response time (s)	Recovery time (s)	Ref.
ZnO	Aqueous solution	300	8	5	15	[20]
ZnO	Hydrothermal	425	5	7	10	[21]
ZnO	Sol-gel	Room temp.	10	19	6	[22]
ZnO	Sol-gel	Room temp.	5	12	7	[22]
ZnO:Au	Wet-chemical	300	0.1	6	24	[23]
ZnO:CuO	Sol-gel	310	0.2	7	10	[24]
ZnO:Al:Pt	Magnetron sputtering	450	10	2.9	–	[25]
ZnO:Al	Hydrothermal	450	10	3	–	[7]
ZnO:Al	Hydrothermal	500	0.1	44	70	[26]
ZnO:Al	Hydrothermal	500	0.5	78	113	[26]
ZnO:Al	Hydrothermal	500	1	147	181	[26]
ZnO:Al	Sol-gel	Room temp.	1	6	32	Present work

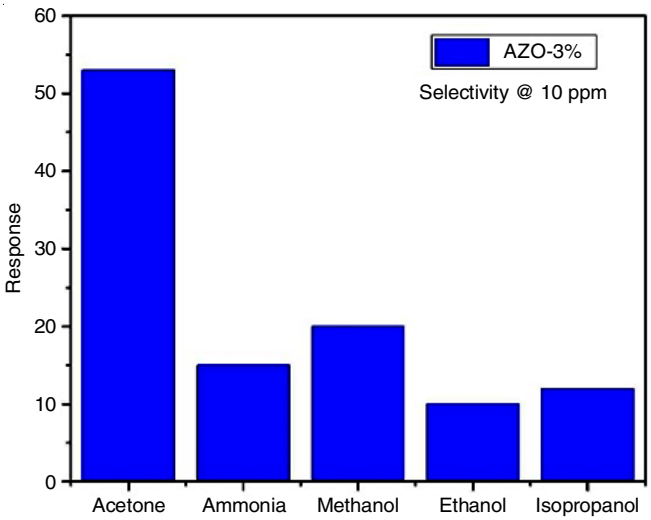

Fig. 7. Response of Al doped ZnO (3 at %) towards 10 ppm of different interfering gases

refers to the duration required for the resistance to reach a stable state subsequent to exposure to acetone gas, whereas the recovery time denotes the duration necessary for the resistance to revert back to its initial value subsequent to the removal of acetone gas.

A fast response time of 6 s was demonstrated by 3% Al-doped ZnO thin film, confirming its capacity to swiftly identify changes in acetone concentration. Additionally, it showed a recovery time of 32 s, showing that once the acetone gas was eliminated, it returned to its initial state quickly. A 3% Al-doped ZnO thin film appears to have good dynamic performance based on these response and recovery durations, making it a potential candidate for real-time acetone gas sensing applications. A comparison between acetone detection in the current investigation and previously published studies is shown in Table-2.

Conclusion

This work investigated the acetone sensing properties of pure and Al-doped ZnO thin films prepared by the sol-gel dip coating method. The primary objective of the experiment was to investigate the impact of varying levels of Al dopant on the structural, morphological and sensing properties of the films. When exposed to 10 ppm of acetone at room temperature, 3 at% Al-doped ZnO thin film showed the highest response at 53%. Moreover, the results of the selectivity tests suggested that the film exhibited a significant level of selectivity towards acetone, even when exposed to several interfering gases. The findings of this study indicate that the sol-gel dip-coated thin films of Al-doped ZnO has promising capabilities for utilization in high-performance acetone gas sensing applications.

CONFLICT OF INTEREST

The authors declare that there is no conflict of interests regarding the publication of this article.

REFERENCES

1. V. Saasa, T. Malwela, M. Mokgotho, C.-P. Liu, B. Mwakikunga and M. Beukes, *Diagnostics*, **8**, 12 (2018); https://doi.org/10.3390/diagnostics8010012
2. Q.A. Drmosh, I. Olanrewaju Alade, M. Qamar and S. Akbar, *Chem. Asian J.*, **16**, 1519 (2021); https://doi.org/10.1002/asia.202100303
3. M. Poloju, N. Jayababu and M.V. Ramana Reddy, *Mater. Sci. Eng. B*, **227**, 61 (2018); https://doi.org/10.1016/j.mseb.2017.10.012
4. V.S. Bhati, M. Hojamberdiev and M. Kumar, *Energy Rep.*, **6**, 46 (2020); https://doi.org/10.1016/j.egyr.2019.08.070
5. A.M. Pineda-Reyes, M.R. Herrera-Rivera, H. Rojas-Chávez, H. Cruz-Martínez and D.I. Medina, *Sensors*, **21**, 4425 (2021); https://doi.org/10.3390/s21134425
6. G. Marinov, K. Lovchinov, V. Madjarova, V. Strijkova, M. Vasileva, N. Malinowski and T. Babeva, *Opt. Mater.*, **89**, 390 (2019); https://doi.org/10.1016/j.optmat.2019.01.055
7. R. Yoo, A.T. Güntner, Y. Park, H.J. Rim, H.-S. Lee and W. Lee, *Sens. Actuators B Chem.*, **283**, 107 (2019); https://doi.org/10.1016/j.snb.2018.12.001
8. M. Sinha, R. Mahapatra, M.K. Mondal, S. Krishnamurthy and R. Ghosh, *Physica E*, **118**, 113868 (2020); https://doi.org/10.1016/j.physe.2019.113868
9. M. Niazmand, A. Maghsoudipour, M. Alizadeh, Z. Khakpour and A. Kariminejad, *Ceram. Int.*, **48**, 16091 (2022); https://doi.org/10.1016/j.ceramint.2022.02.155
10. Y.-S. Kim and W.-P. Tai, *Appl. Surf. Sci.*, **253**, 4911 (2007); https://doi.org/10.1016/j.apsusc.2006.10.068
11. S. Motloung, F.B. Dejene, R.E. Kroon, H.C. Swart and O.M. Ntwaeaborwa, *Physica B*, **468**-469, 11 (2015); https://doi.org/10.1016/j.physb.2015.04.007
12. M.R. Islam, M. Rahman, S.F.U. Farhad and J. Podder, *Surf. Interfaces*, **16**, 120 (2019); https://doi.org/10.1016/j.surfin.2019.05.007

13. J.H. Lee, C.-Y. Chou, Z. Bi, C.-F. Tsai and H. Wang, *Nanotechnology*, **20**, 395704 (2009); https://doi.org/10.1088/0957-4484/20/39/395704
14. F. Giovannelli, C. Chen, P. Díaz-Chao, E. Guilmeau and F. Delorme, *J. Eur. Ceram. Soc.*, **38**, 5015 (2018); https://doi.org/10.1016/j.jeurceramsoc.2018.07.032
15. W. Khan, Z.A. Khan, A.A. Saad, S. Shervani, A. Saleem and A.H. Naqvi, *Int. J. Modern Phys.: Conf. Ser.*, **22**, 630 (2013); https://doi.org/10.1142/S2010194513010775
16. Q. You, H. Cai, Z. Hu, P. Liang, S. Prucnal, S. Zhou, J. Sun, N. Xu and J. Wu, *J. Alloys Compd.*, **644**, 528 (2015); https://doi.org/10.1016/j.jallcom.2015.05.060
17. S. Khlayboonme and W. Thowladda, *Mater. Res. Express*, **8**, 076402 (2021); https://doi.org/10.1088/2053-1591/ac113d
18. J. Dai, Z. Suo, Z. Li and S. Gao, *Results Phys.*, **15**, 102649 (2019); https://doi.org/10.1016/j.rinp.2019.102649
19. R. Tian, Z. Gao, R. Lang, N. Li, H. Gu, G. Chen, H. Guan, E. Comini and C. Dong, *J. Nanostructure Chem.*, (2022); https://doi.org/10.1007/s40097-022-00475-4
20. Y. Zeng, T. Zhang, M. Yuan, M. Kang, G. Lu, R. Wang, H. Fan, Y. He and H. Yang, *Sens. Actuators B Chem.*, **143**, 93 (2009); https://doi.org/10.1016/j.snb.2009.08.053
21. M.R. Alenezi, S.J. Henley, N.G. Emerson and S.R.P. Silva, *Nanoscale*, **6**, 235 (2014); https://doi.org/10.1039/C3NR04519F
22. K. Muthukrishnan, M. Vanaraja, S. Boomadevi, R.K. Karn, V. Singh, P.K. Singh and K. Pandiyan, *J. Alloys Compd.*, **673**, 138 (2016); https://doi.org/10.1016/j.jallcom.2016.02.222
23. F. Meng, N. Hou, Z. Jin, B. Sun, W. Li, X. Xiao, C. Wang, M. Li and J. Liu, *Sens. Actuators B Chem.*, **219**, 209 (2015); https://doi.org/10.1016/j.snb.2015.04.132
24. Y. Xie, R. Xing, Q. Li, L. Xu and H. Song, *Sens. Actuators B Chem.*, **211**, 255 (2015); https://doi.org/10.1016/j.snb.2015.01.086
25. A. Koo, R. Yoo, S.P. Woo, H.S. Lee and W. Lee, *Sens. Actuators B Chem.*, **280**, 109 (2019); https://doi.org/10.1016/j.snb.2018.10.049
26. R. Yoo, Y. Park, H. Jung, H. Rim, S. Cho, H. Lee and W. Lee, *J. Alloys Compd.*, **803**, 135 (2019); https://doi.org/10.1016/j.jallcom.2019.06.254